ChemElectroChem

Supporting Information

Engineering ORR Electrocatalysts from Co_8Pt_4 Carbonyl Clusters via ZIF-8 Templating

Peter M. Schneider, Kathrin L. Kollmannsberger, Cristiana Cesari, Rachit Khare, Maxime Boniface, Beatriz Roldán Cuenya, Thomas Lunkenbein, Martin Elsner, Stefano Zacchini, Aliaksandr S. Bandarenka,* Julien Warnan,* and Roland A. Fischer*

Supporting Information

Engineering ORR Electrocatalysts from Co_8Pt_4 Carbonyl Clusters via ZIF-8 Templating

Peter M. Schneider †, Kathrin L. Kollmannsberger †, Cristiana Cesari, Rachit Khare, Maxime Boniface, Beatriz Roldán Cuenya, Thomas Lunkenbein, Martin Elsner, Stefano Zacchini, Aliaksandr S. Bandarenka,* Julien Warnan,* and Roland A. Fischer*

Outline

1. General Information

All chemicals were purchased from commercial suppliers and used without purification. *Schlenk* technique and the glove box were used for carrying out the reactions under argon atmosphere. If necessary, the solvents were dried *via* the *MBraun MB SPS* purification system, additionally degassed using 15 ultrasonication cycles and stored over molecular sieves (3 or 4 Å).

Transmission and scanning electron microscopy measurements. HR-TEM and HAADF-STEM images were acquired using a JEOL ARM200F microscope operated at 200 kV. STEM measurements were carried out with a convergence angle of 22.8 mrad and a beam current of 22.5 pA. Supported cluster samples were directly prepared by drop-casting on TEM grids with lacey carbon support films. Prior to imaging the samples were subjected to electron beam shower in TEM mode to reduce carbon contamination. Statistical size analysis was carried out using ImageJ. In addition, TEM images were recorded with a *Jeol* JEM 1400plus operated at 120 kV. SEM images were obtained with a *Jeol* JSM-7500F field emission scanning electron microscope.

X-ray emission spectroscopy (XES) measurements. X-ray emission spectroscopy (XES) measurements were collected at the ID26 beamline of the European Synchrotron Radiation Facility (ESRF) in Grenoble, France. The storage ring operated at ~6 GeV energy and ~90 mA current. A flat Si(311) DCM was used for obtaining monochromatic X-rays and a Si-coated plane mirror was used for rejecting higher harmonics. The DCM was calibrated by measuring a Co-foil and defining the first inflection point as 7709 eV.

Co $K\alpha_1$ High energy resolution fluorescence detected X-ray absorption near edge structure (HERFD-XANES) spectra were collected using a Johann-type XES spectrometer equipped with two Si(531) crystals placed on a five-analyzer crystal XES spectrometer and a dead-time corrected avalanche photodiode (APD) detector. The Si(531) crystals were used to select the Co $K\alpha_1$ emission energy

(~6930 eV). Spectra were then measured between 7680 eV and 7830 eV incident energy with a step size of 0.2 eV. Possible attenuation in emission signal was reduced by placing a He-filled balloon inside the Rowland circle between the sample, the analyzer crystals, and the detector. The data were monitored for any signs of beam damage and several scans were averaged to reduce the signal-to-noise ratio and improve the data quality.

X-ray Photoelectron Spectroscopy (XPS). X-ray photoelectron spectroscopy (XPS) spectra of the $Pt_{27}Co_1$/C catalyst were conducted on a SPECS setup (SPECS XR50 Xf-Ray source, a SPECS PHOIBOS 150 hemispherical analyzer and SPECS spectrometer) using a non-monochromatized Al K_α source (1486.7 eV). 40 µL of the catalyst ink were drop-casted on a glassy carbon disk and let dried. XPS spectra of the thin catalyst ink film on glassy carbon were recorded before and after the electrochemical activity measurement protocol. All spectra were acquired in an ultra-high vacuum chamber at an operating pressure below 5 x 10^{-9} mbar. The data was analyzed with the Casa XPS software (Version 2.3.24PR1.0). The binding energies were corrected by referencing the C-C peak of the C 1s spectrum to 284.5 eV.

Elemental Analysis. The Elemental Analyzer (*Euro EA*) was used to quantify C, H, N, S *via* flash combustion and subsequent chromatographic separation. Zn and Sn were analyzed by AAS (Atomic Absorption Spectroscopy) utilizing an *Agilent Technologies 200* (280FS AA) while Pt, and Co are analyzed photometrically applying *Agilent Technologies Cary Serie UV-Vis Spectrophotometer* (Cary 100 UV-Vis).

Inductively coupled plasma mass spectrometry. To obtain an accurate quantification of the Pt and Co amount ICP-MS for platinum and Co respectively was conducted on a *Perkin Elmer NexIon* 350D ICP-MS instrument. ^{195}Pt and ^{59}Co were used as target masses for the analytes and ^{103}Rh for internal standard. Analyte quantification was carried out in standard mode with correction equation to avoid polyatomic interferences. External Calibration was performed in the range of 0 µg L^{-1} to 100 µg L^{-1}. Each sample was measured with five measurement replicates, a dwell time per 50 ms and an integration time of 750 ms. For the samples preparation (m≈1 mg) were weight with a micro scale, digested with freshly prepared aqua regia, heated to 80 °C, diluted with Milli-Q®water, filtered over silica and again diluted to meet the calibrated concentration range.

Electrocatalytic testing. For the rotating disk electrode (RDE) measurements, a RDE instrument and glassy carbon RDE tips with 5 mm diameter purchased from *OrigaLys ElectroChem SAS* were used. BioLogic VSP-300 potentiostat (*BioLogic*, France) was used for all of the electrochemical techniques. For the measurements, 2 mg of the catalyst material were dispersed in 713 µL of ultra-pure Milli-Q® water (18.2 MΩcm, *Merck Millipore*, USA), 289 µL isopropanol (puriss. p.a., ACS reagent, ≥ 99.8%, *Sigma Aldrich*, USA) and 6 µL of Nafion (5 wt% in lower aliphatic alcohols and water, Sigma Aldrich, USA), and sonicated for 20-30 min. 10 µL of this suspension were deposited on a glassy carbon electrode and dried under continuous rotation at 300 rpm to obtain a homogeneous coating of the

catalyst. Prior to the electrochemical measurements, the glassy carbon tip was polished with 1, 0.3, and 0.05 μm alumina paste, respectively, and rinsed with ultra-pure water. Cyclic voltammograms were recorded in Ar-saturated (5.0, *Westfalen*, Germany) 0.1 M $HClO_4$ solution (prepared from 70% $HClO_4$, extra pure, Acros, Germany) with a scan rate of 50 mVs^{-1} in order to electrochemically clean the catalyst surface. For ORR activity measurements, O_2-saturated (4.5, *Westfalen*, Germany) 0.1 M $HClO_4$ was used as an electrolyte. The scan range for the CVs in Ar- and O_2-saturated electrolytes was selected from 0.07 V to 1.0 V vs RHE. In all RDE measurements, Pt wire and mercury/mercurous sulfate (MMS, *SI Analytics*, Germany) were used as counter and reference electrode, respectively. All reported potentials in this work are referred vs RHE. The conversion from MMS to RHE potential scale was done by calibrating the MMS reference electrode in H_2-saturated 0.1 M $HClO_4$ by measuring the intercept of the hydrogen oxidation/evolution curve with the x-axis. The intercept refers to the conversion potential specific for the MMS reference electrode and 0.1 M $HClO_4$ electrolyte solution used in our experiments (typically ~ -0.719 V vs MMS).

Here, the term electrochemical activation means the performing of cyclic voltammograms for >350 cycles under the just described conditions. Mass activity was determined utilizing the Pt loadings obtained through the ICP-MS by normalizing the kinetic current determined at 0.9 V vs RHE to the Pt loading on the glassy carbon electrode. The kinetic current was derived from the polarization curve according to the equation: $|i_k| = (|i| \times |i_L|)/(|i_L| - |i|)$, where i_k, i_L, and i represent the kinetic current, diffusion-limited current and measured current, respectively. The electroactive surface area (ECSA) of the Pt-based nanoparticles was determined by hydrogen underpotential deposition (HUPD) from the cyclic voltammogram under Ar-saturation between 0.1 and 0.4 V vs RHE. The integrated charge of the peaks was normalized to the assumed total charge of 210 $\mu C/cm^2$ for a monolayer of hydrogen adsorption on Pt. Normalizing the ECSA to the Pt weight loading on the glassy carbon electrode results in the specific surface area (SSA) of the synthesized catalysts.

X-ray diffraction. PXRD measurements were performed on a silicon single-crystal wafer using *Bragg Brentano* geometry in a *Rigaku* MiniFlex 600-C diffractometer. X-ray Cu Kα radiation (λ_1 - 1.5406 Å, λ_2 - 1.5444 Å, I_2/I_1 - 0.5) was used, and K_β radiation was removed by a Ni-filter. The measurement range, unless stated otherwise, was from 2.0° to 50.0/90.0° (2θ) with a step size of 0.010 degrees and a scan rate of 5 degrees per minute.

2. Characterization

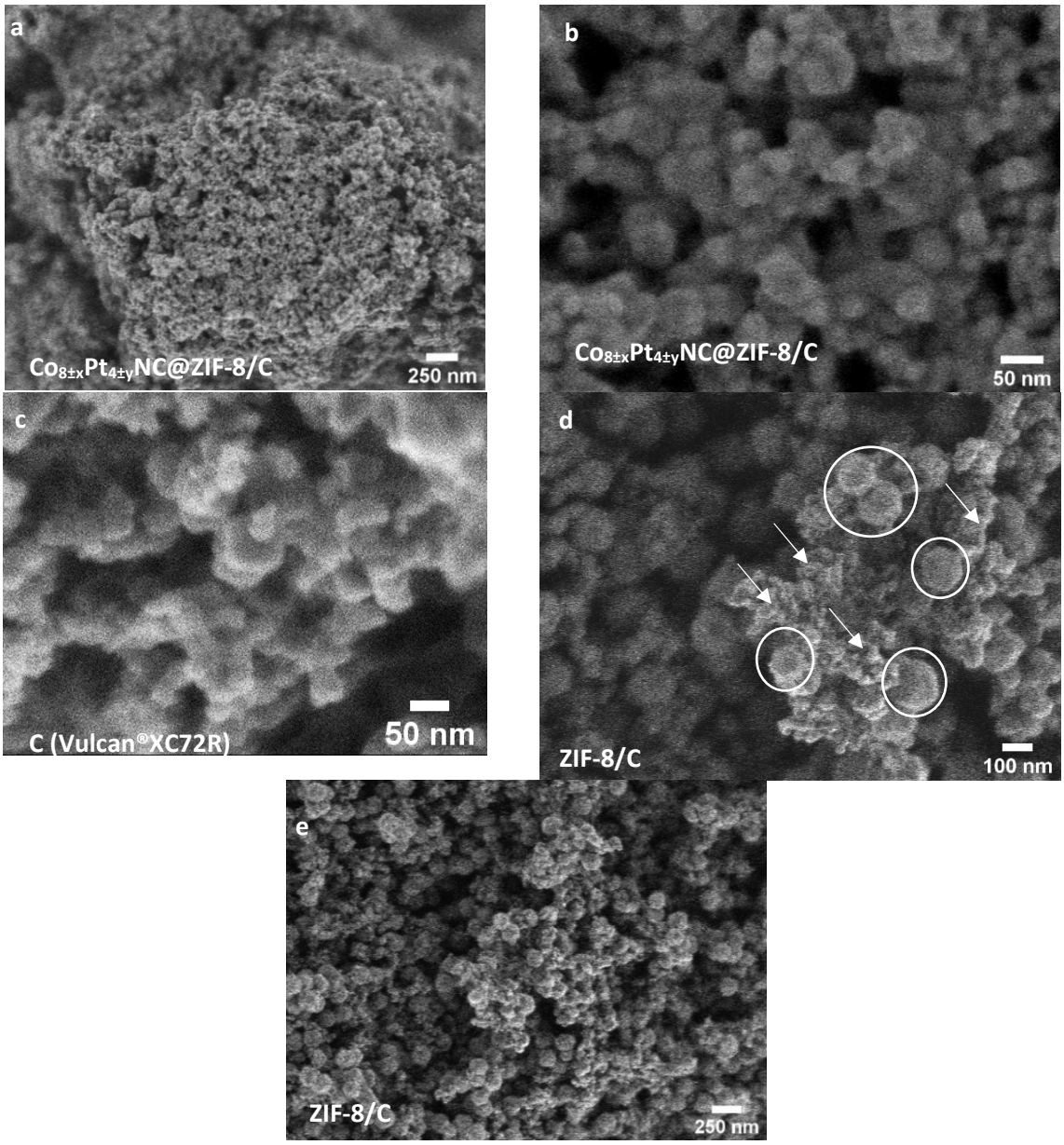

Figure S1: SEM (**a**, **b**) images of $Co_{8\pm x}Pt_{4\pm y}$NC@ZIF-8/C (carbon black which equals Vulcan® XC72R). SEM images of ZIF-8(d~100 nm)/C (d~20 nm) (**c**, **d** with arrows and circles marking ZIF-8 and C, respectively), revealing mixing of both components, and pure Vulcan®XC72R (**e**).

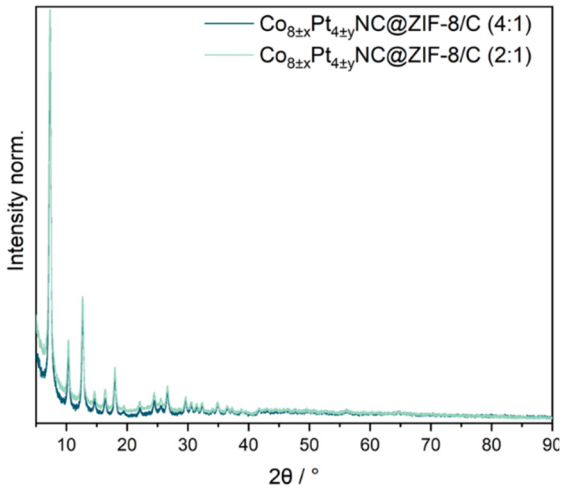

Figure S2: PXRD patterns of the hybrid material $Co_{8\pm x}Pt_{4\pm y}NC$@ZIF-8/C with two different stoichiometries.

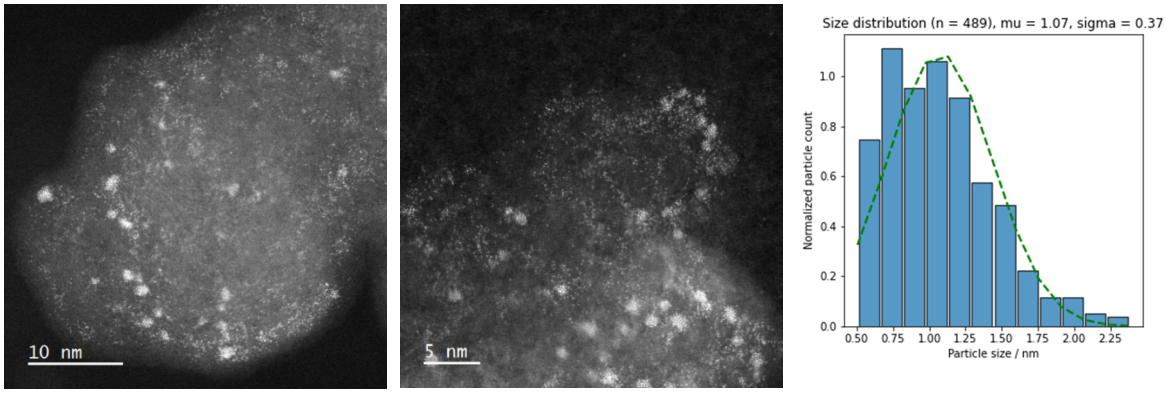

Figure S3: HAADF-STEM images of $Pt_{27}Co_1$/C before the electrochemical measurements. White arrows highlight exemplarily two Pt single atoms. The histogram depicts the size distribution.

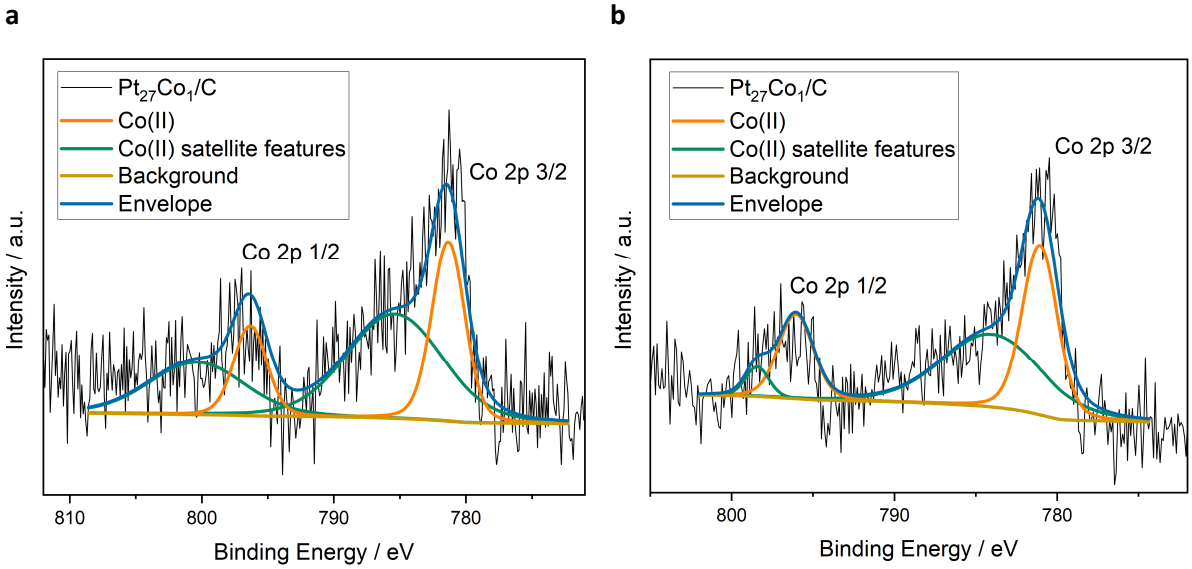

Figure S4: Fitted XPS spectra of the Co 2p core-level region of $Pt_{27}Co_1$/C. Co 2p spectra were only acquired before cycling and for two different spots on the sample.

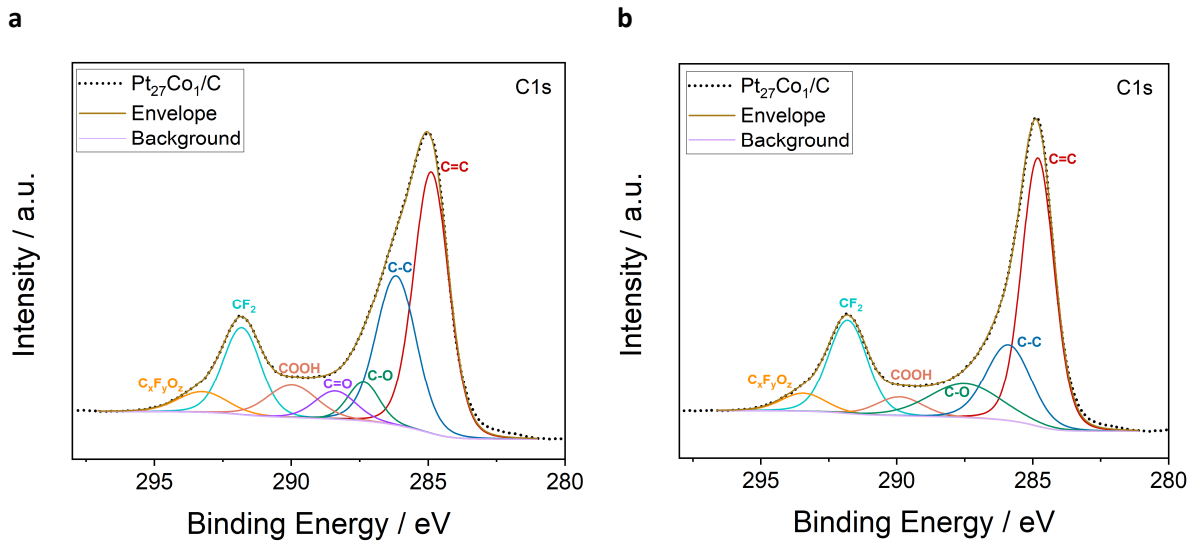

Figure S5: Fitted XPS spectra of the C 1s core-level region of $Pt_{27}Co_1/C$ a before and b after electrochemical cycling.

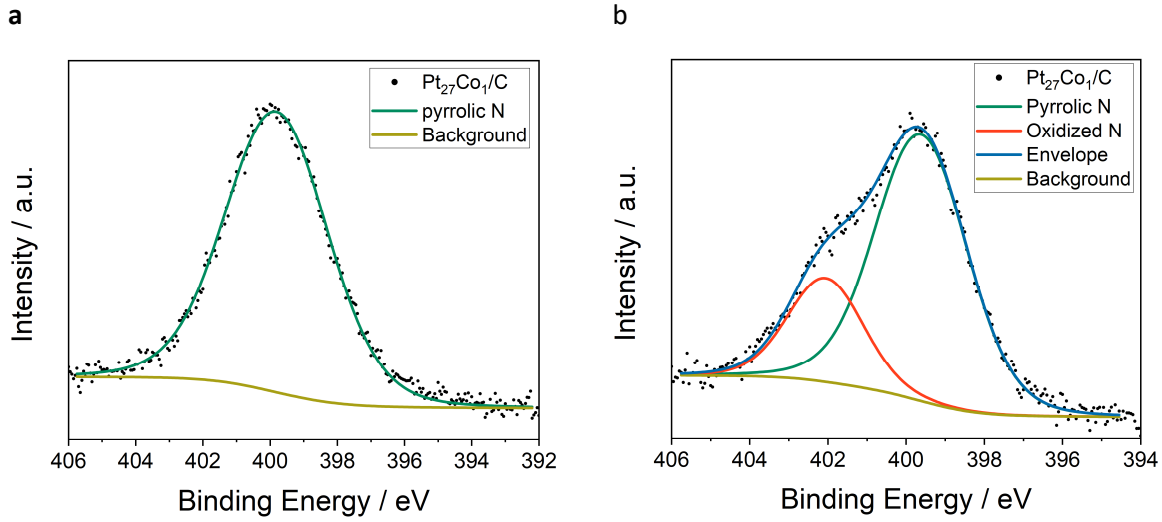

Figure S6: Fitted XPS spectra of the N 1s core-level region of the $Pt_{27}Co_1/C$ **a** before and **b** after electrochemical cycling.

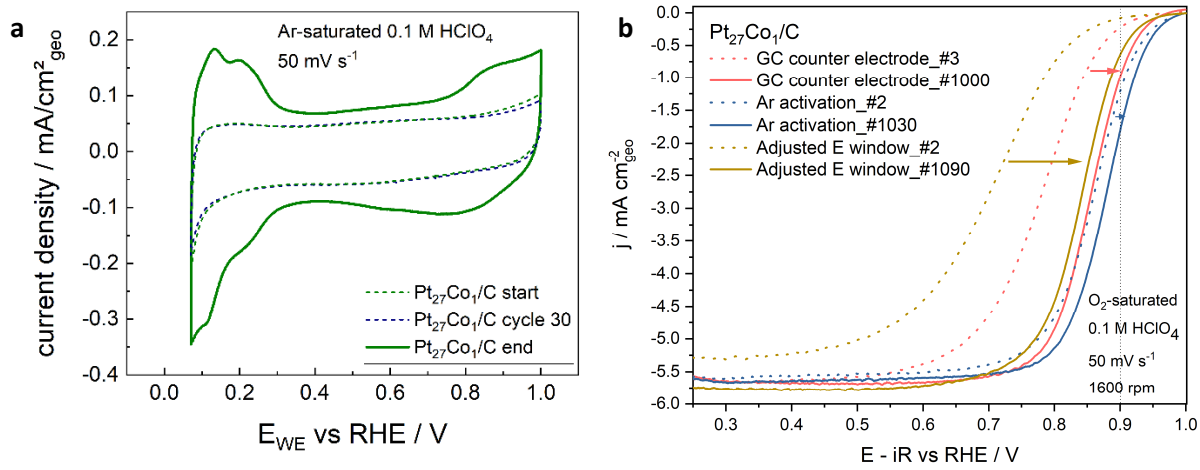

Figure S7: (**a**) Typical CVs of $Pt_{27}Co_1/C$ in Ar-saturated 0.1 M $HClO_4$ at a scan rate of 50 mV s^{-1} in the beginning (green dotted curve), after typical catalyst activation and stabilization (30 cycles, blue dotted curve), and in the end (solid curve) of the electrochemical examination, normalized to the geometric surface area of the glassy carbon electrode (0.196 cm^2). (**b**) Catalyst activation tests revealing an activity increase with cycling not only under standard conditions but also **i)** with glassy carbon counter electrode, **ii)** when cycling in Ar-saturated 0.1 M $HClO_4$ and **iii)** with adjusted potential window during cycling (0.06 V vs RHE to 1.1 V vs RHE).

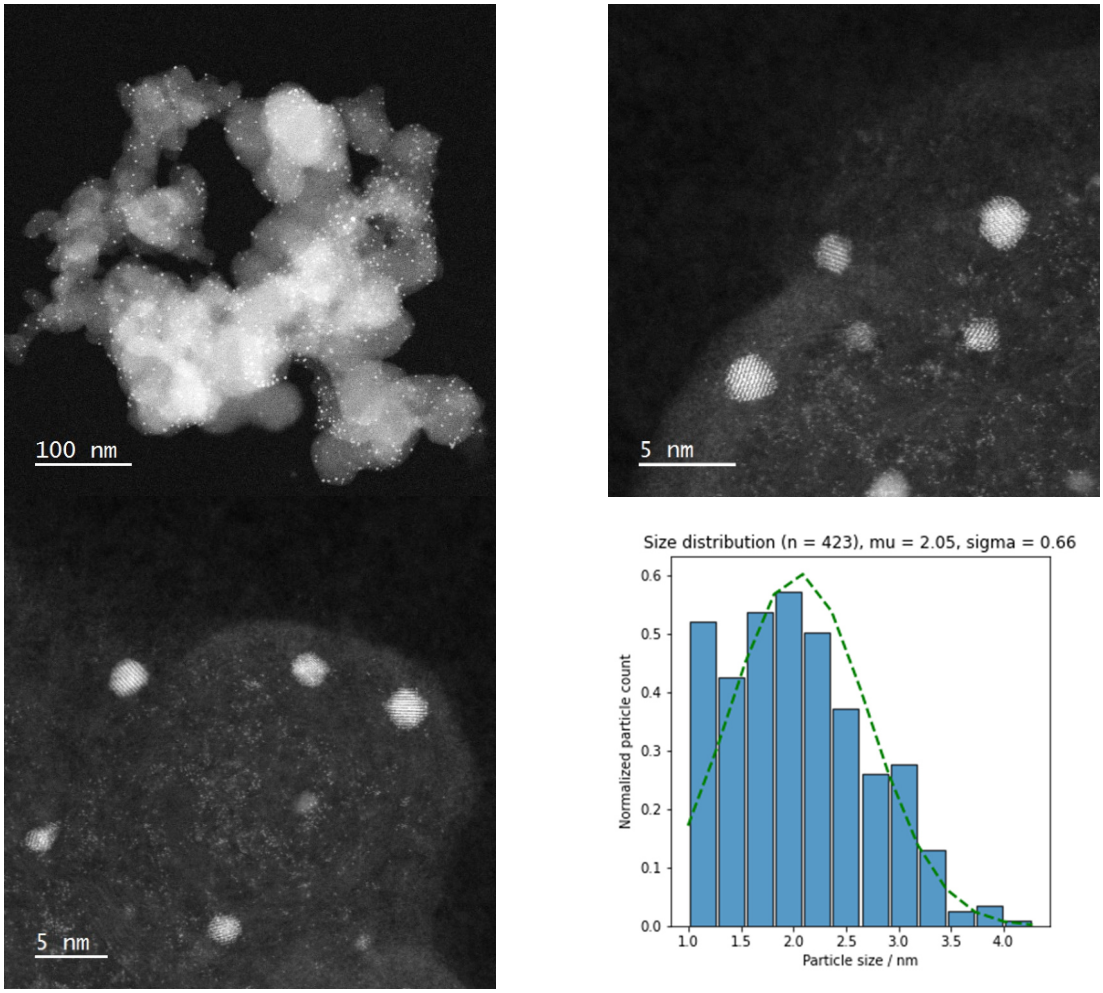

Figure S8: HAADF-STEM images of $Pt_{27}Co_1/C$ after the electrochemical measurements revealing bigger NPs; Histograms depicts the size-distribution.

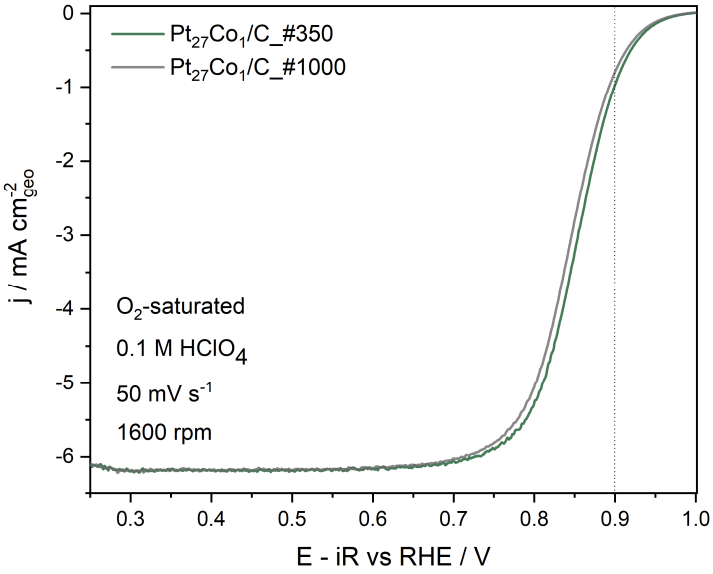

Figure S9: Polarization curve of $Pt_{27}Co_1/C$ after #350 and #1000 CV cycles.

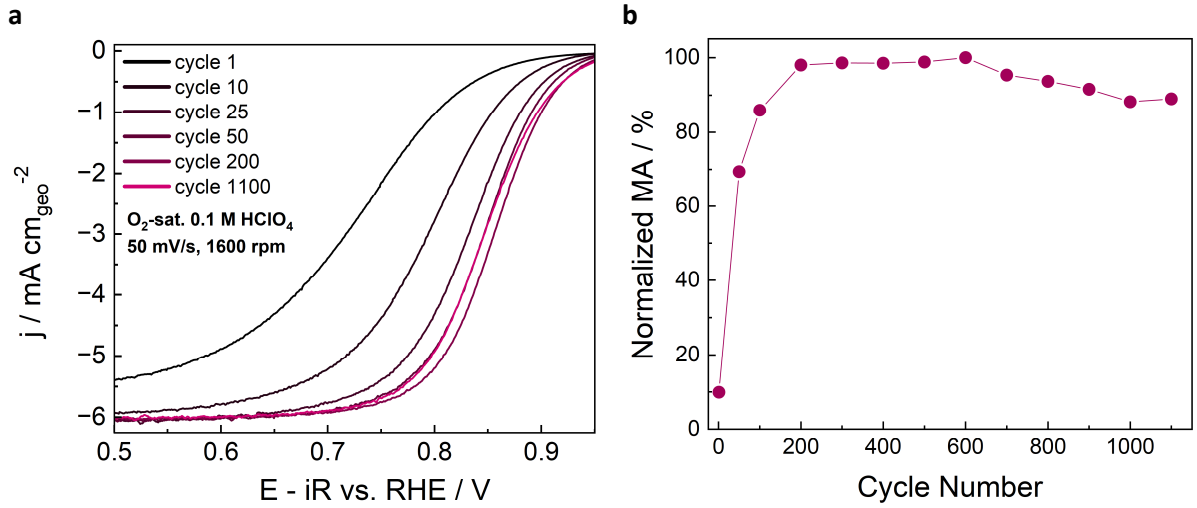

Figure S10: (**a**) evolution of an exemplary ORR polarization curve of $Pt_{27}Co_1/C$ over 1100 cycles. (**b**) Evolution of the mass activity, calculated from (**a**). The plotted mass activities were normalized to the maximum mass activity for better visualization.

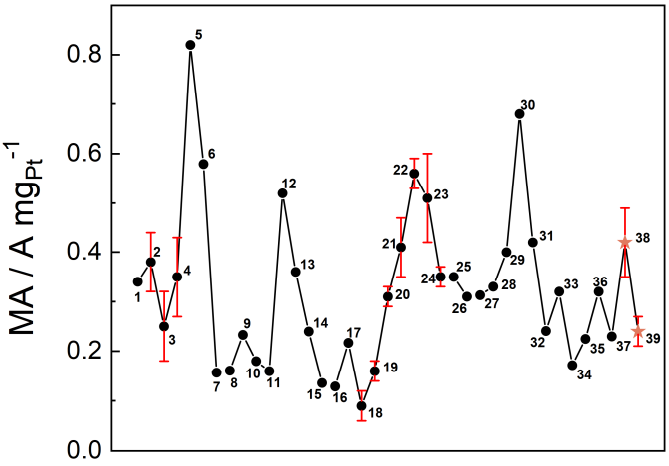

Figure S11: Comparison of the mass activities of various Pt/C and PtCo/C catalyst systems from the literature (Number 1-37). Numbers 38 and 39 represent $Pt_{27}Co_1$/C via ZIF-8 and Co_8Pt_4 NC@Vulcan from this work, respectively. The numbers in the figure refer to the sample numbers from Table S2. Detailed information of the samples is shown in Table S2.

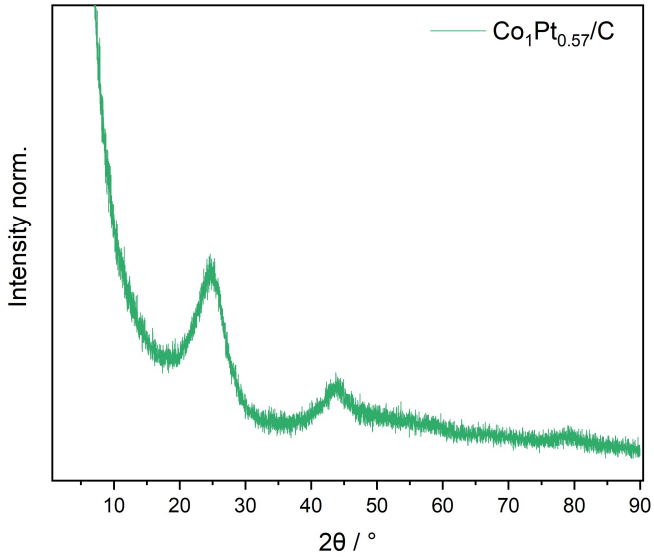

Figure S12: PXRD of $Co_1Pt_{0.57}$/C without visible NP reflections.

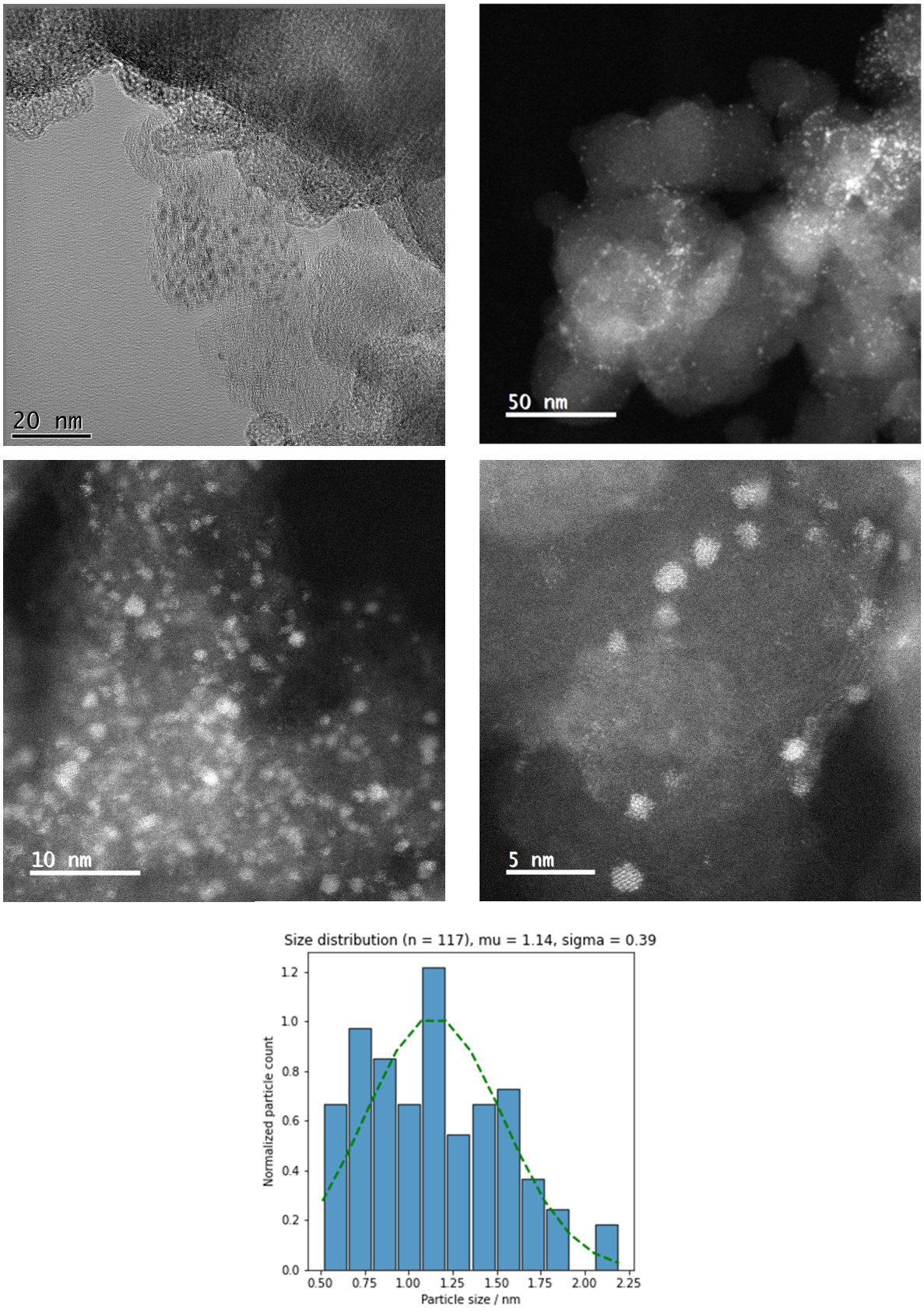

Figure S13: HR-TEM and HAADF-STEM images of $Pt_1Co_{0.57}/C$ obtained through direct cluster deposition and activation; Histograms depicts the size-distribution.

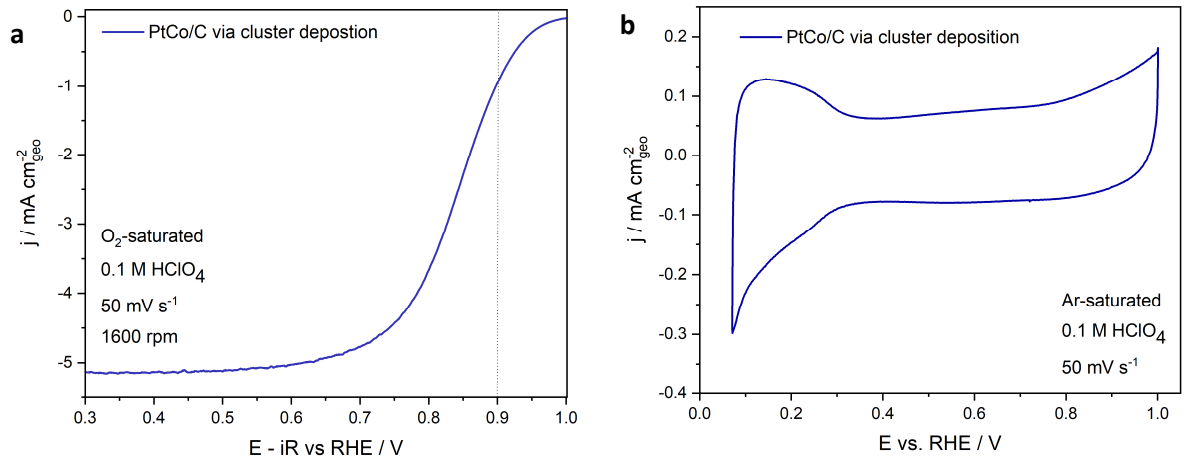

Figure S14: **a** Polarisation curve and **b** CV of $Pt_1Co_{0.57}$/C obtained *via* direct cluster deposition and activation.

Note	Core level	$BE_{measured}$ [eV]	$BE_{literature}$ [eV]
before cycling	Pt $4f_{7/2}$ (II)	72.8	72.2
	Pt $4f_{7/2}$ (IV)	75.2	74.5
before cycling, spot 1	Co $2p_{3/2}$ (II)	781.4	780.0
	Co $2p_{3/2}$ sat. features	785.8	~786
before cycling, spot 2	Co $2p_{3/2}$ (II)	781.1	780.0
	Co $2p_{3/2}$ sat. features	784.3	~ 786
after cycling	Pt $4f_{7/2}$ (0)	71.3	71.0
	Pt $4f_{7/2}$ (II)	72.8	72.2
	Pt $4f_{7/2}$ (IV)	74.2	74.5

Table S1: Summary of the binding energy (BE) peak positions of Pt 4f and Co 2p spectra. Pt 4f spectra were recorded before and after the electrochemical cycling. Co 2p spectra were only acquired before cycling and for two different spots on the sample. Reference peak positions of various Pt 4f and Co 2p states from the literature were added for comparison.[1],[2],[3]

Number	Catalyst	Electrolyte	MA [A mg_{Pt}^{-1}]		Ref.
1	$PtCo_3$	0.1 M $HClO_4$	0.34	@ 0.9 V vs RHE	[4]
2	$PtCo_3$	0.1 M $HClO_4$	0.38 ± 0.06	@ 0.9 V vs RHE	[5]
3	PtCo	0.1 M $HClO_4$	0.25 ± 0.07	@ 0.9 V vs RHE	[5]
4	Pt_3Co	0.1 M $HClO_4$	0.35 ± 0.08	@ 0.9 V vs RHE	[5]
5	PtCo@NC-10	0.1 M $HClO_4$	0.82	@ 0.9 V vs RHE	[6]
6	Co-doped Pt	0.1 M $HClO_4$	0.579	@ -	[7]
7	$Pt_{93}Co$/C	0.1 M $HClO_4$	0.157	@ 0.9 V vs RHE	[8]
8	$Pt_{82}Co$/C	0.1 M $HClO_4$	0.161	@ 0.9 V vs RHE	[8]
9	$Pt_{36}Co$/C	0.1 M $HClO_4$	0.233	@ 0.9 V vs RHE	[8]
10	$Pt_{31}Co$/C	0.1 M $HClO_4$	0.180	@ 0.9 V vs RHE	[8]
11	Pt_3Co/C-400	0.1 M $HClO_4$	0.16	@ 0.9 V vs RHE	[9]
12	Pt_3Co/C-700	0.1 M $HClO_4$	0.52	@ 0.9 V vs RHE	[9]
13	PtCo	0.1 M $HClO_4$	0.36	@ 0.9 V vs RHE	[10]
14	Pt_3Co	0.1 M $HClO_4$	0.24	@ 0.9 V vs RHE	[10]
15	Pt_3Co	0.1 M $HClO_4$	0.136	@ 0.9 V vs RHE	[11]
16	Pt_3Co@200°C	0.1 M $HClO_4$	0.129	@ 0.9 V vs RHE	[11]
17	Pt_3Co@500°C	0.1 M $HClO_4$	0.217	@ 0.9 V vs RHE	[11]
18	$PtCo_{2.7}$/C	0.1 M $HClO_4$	0.09 ± 0.03	@ 0.9 V vs RHE	[12]
19	$PtCo_{3.4}$/C-350°C	0.1 M $HClO_4$	0.16 ± 0.02	@ 0.9 V vs RHE	[12]
20	$PtCo_{3.0}$/C-600°C	0.1 M $HClO_4$	0.31 ± 0.02	@ 0.9 V vs RHE	[12]
21	$PtCo_{2.7}$/C-700°C	0.1 M $HClO_4$	0.41 ±0.06	@ 0.9 V vs RHE	[12]
22	$PtCo_{3.0}$/C-800°C	0.1 M $HClO_4$	0.56 ±0.03	@ 0.9 V vs RHE	[12]
23	$PtCo_{2.8}$/C-900°C	0.1 M $HClO_4$	0.51 ±0.09	@ 0.9 V vs RHE	[12]
24	$PtCo_{2.8}$/C-1000°C	0.1 M $HClO_4$	0.35 ±0.02	@ 0.9 V vs RHE	[12]
25	Pt_3Co acid-treated	0.1 M $HClO_4$	0.35	@ 0.9 V vs RHE	[13]
26	Pt_3Co annealed	0.1 M $HClO_4$	0.31	@ 0.9 V vs RHE	[13]
27	PtCo/C	0.1 M $HClO_4$	0.313	@ 0.9 V vs RHE	[14]
28	PtCo/C-TKK	0.1 M $HClO_4$	0.33	@ 0.9 V vs RHE	[15]
29	PtCo/C-450	0.1 M $HClO_4$	0.40	@ 0.9 V vs RHE	[15]
30	PtCo/C-600	0.1 M $HClO_4$	0.68	@ 0.9 V vs RHE	[15]
31	Pt/C TKK 20 wt.-%	0.1 M $HClO_4$	0.42	@ 0.9 V vs RHE	[16]
32	Pt/C TKK 20 wt.-%	0.1 M $HClO_4$	0.241	@ 0.9 V vs RHE	[7]
33	Pt/C TKK 60 wt.-%	0.1 M $HClO_4$	0.32	@ 0.9 V vs RHE	[17]
34	Pt/C E-TEK	0.1 M $HClO_4$	0.172	@ 0.9 V vs RHE	[18]
35	PtC HiSPEC 3000	0.1 M $HClO_4$	0.225	@ 0.9 V vs RHE	[19]
36	PtC HiSPEC 4000	0.1 M $HClO_4$	0.32	@ 0.9 V vs RHE	[19]
37	PtC HiSPEC 9100	0.1 M $HClO_4$	0.23	@ 0.9 V vs RHE	[19]
38	$Pt_{27}Co_1$/C *via* ZIF-8	0.1 M $HClO_4$	0.42 ± 0.07	@ 0.9 V vs RHE	-
39	Co_8Pt_4 NC@Vulcan	0.1 M $HClO_4$	0.24 ± 0.03	@ 0.9 V vs RHE	-

Table S2: Detailed information on the MA of various PtCo and non-noble metal catalysts provided in the literature. For comparison, only catalyst nanostructures supported on carbon are included herein. Numbers 38 and 39 are from this work.

3. References

[1] J. S. Hammond, N. Winograd, *J. Electroanal. Chem.* **1977**, 78, 55-69
[2] T. J. Chuang, C. R. Brundle, D. W. Rice, *Surf. Sci.* **1976**, 59, 413-429
[3] N. S. McIntyre, M. G. Cook, *Anal. Chem.* **1975**, 47, 2208-2213
[4] R. Srivastava, P. Mani, N. Hahn, P. Strasser, *Angew. Chem. Int. Ed.* **2007**, 46, 8988
[5] M. Oezaslan, F. Hasché, P. Strasser, *J. Electrochem. Soc.* **2012**, 159, B394
[6] N. Du, C. Wang, R. Long, Y. Xiong, *Nano Res.* **2017**, 10, 3228
[7] X. Duan, F. Cao, R. Ding, X. Li, Q. Li, R. Aisha, S. Zhang, K. Hua, Z. Rui, Y. Wu, J. Li, A. Li, J. Liu, *Adv. Energy Mater.* **2022**, 12, 2103144
[8] X. Tang, D. Fang, L. Qu, D. Xu, X. Qin, B. Qin, W. Song, Z. Shao, B. Yi, *Chinese J. Catal.* **2019**, 40, 504-514
[9] D. Wang, H. L. Xin, R. Hovden, H. Wang,Y. Yu, D. A. Muller, F. J. DiSalvo, H. D. Abruna, *Nature Mater.* **2013**, 12, 81
[10] N. M. Marković, T. J. Schmidt, V. Stamenković, P. N. Ross, *Fuel Cells* **2001**, 1, 104-11
[11] Z. Liu, C. Yu, I. A. Rusakova, D. Huang, P. Strasser, *Top. Catal.* **2008**, 49, 241-250
[12] H. Schulenburg, E. Müller, G. Khelashvili, T. Roser, H. Bönnemann, A. Wokaun, G. G. Scherer, *J. Phys. Chem. C* **2009**, 113, 4069-4077
[13] S. Chen, P. J. Ferreira, W. Sheng, N. Yabuuchi, L. F. Allard, Y. Shao-Horn, *J. Am. Chem. Soc.* **2008**, 130, 13818-13819
[14] Y.-J. Wang, N. Zhao, B. Fang, H. Li, X. T. Bi, H. Wang, *RSC Adv.* **2016**, 6, 34484
[15] H. Zhong, H. Wu, Y. Pan, H. Li, Y. Peng, D. Banham, J. Zeng, *Int. J. Hydrog. Energy* **2022**, 47, 40952-40960
[16] J. Fichtner, B. Garlyyev, S. Watzele, H. A. El-Sayed, J. N. Schwämmlein, W.-J. Li, F. M. Maillard, L. Dubau, J. Michalička, J. M. Macak, A. Holleitner, A. S. Bandarenka, *ACS Appl. Mater. Interfaces* **2019**, 11, 5129-5135
[17] C. Roy, B. P. Knudsen, C. M. Pedersen, A. Velázquez-Palenzuela, L. H. Christensen, C. D. Damsgaard, I. E. L. Stephens, I. Chorkendorff, *ACS Catal.* **2018**, 8, 2071-2080
[18] M. Zhang, Y. Dai, J.-Y. Hu, S. Miao, B.-Q. Xu, *J. Phys. Chem. C* **2021**, 125, 27199-27206
[19] Y. Lv, H. Liu, J. Li, J. Chen, Y. Song, *J. Electroanal.* **2020**, 870, 114172